ELSEVIER

Applied Mathematical Modelling 22 (1998) 1023–1036

APPLIED MATHEMATICAL MODELLING

Particle transport in a bottom-feed separation vessel

Yuguo Li [a], Murray Rudman [a,*], Gary Brown [b]

[a] *CSIRO Building, Construction and Engineering, P.O. Box 56, Highett, Victoria 3190, Australia*
[b] *Alcoa of Australia Limited, P.O. Box 161, Kwinana, W.A. 6167, Australia*

Received 1 July 1997; received in revised form 21 January 1998; accepted 26 February 1998

Abstract

A two-dimensional, axisymmetric numerical model of particle separation in a bottom-feed separation vessel is presented. The model includes six separate particle classes and assumes that the settling velocity of each particle class is sufficiently small when compared to the high inflow turbulence levels that the effect of the particles on turbulence can be neglected. Low particle settling velocities coupled with low particle volume fractions allows application of a drift-flux multi-phase model. The comparison between numerical results and measured plant data is in good agreement for overflow of all particle classes. Results of simulations show that bottom feeding results in a negatively buoyant, particle-laden jet being formed in the core of the vessel. The fraction of large particles that is carried out through the overflow is found to be critically dependent on the inlet velocity. The most effective way to reduce carry-over of large particles at the same time as maintaining through-put is to increase the diameter of the inlet feed pipe.

Keywords: Particle separation; Drift-flux model; Multi-phase flow; Finite-volume method; CFD modelling

1. Introduction

The separation of solids from liquid is an important part of many minerals processing applications and is undertaken in a wide variety of devices including hydro-cyclones, washers, thickeners and classifiers. Often the object of solid–liquid separation is to remove particles of a certain size or density from a polydispersed particulate system, leaving others with different size or density behind in the liquid. In practical applications there is nearly always a spectrum of particle sizes, and often a range of particle densities, in the system. These factors make numerical simulation difficult. For good representation of the particulate system, each different particle size and density combination should be treated individually. In practice this is not feasible, which means that the particle size distribution must be reduced to a few representative particle classes, typically no more than two.

The study presented here originated from an industrial application in which there was a need to separate large particles from a solid–liquid suspension because their presence in the process stream had the potential to adversely affect downstream operations. The desired outcomes were design modifications to a bottom-feed separation vessel that would reduce as much as possible the

* Corresponding author. Tel.: +61 3 9252 6000; fax: +61 3 9252 6244.

0307-904X/98/$ – see front matter
PII: S0307-904X(98)10035-5

percentage of large particles in the overflow. Constraints arising from economic cost, existing plant layout and potential process down-time meant that totally new plant could not be installed and that any modifications must be relatively simple to implement. Plant measurements had been made of particle concentration in the underflow and overflow of the vessel and were presented in terms of six particle sizes, all with the same nominal density. The plant data provided an excellent source of data for model validation.

This paper presents a two-dimensional, axisymmetric numerical model of the particle–liquid flow in such a bottom-feed separation vessel. Numerical simulations together with some fundamental understanding of negatively buoyant jets in an enclosure have made it possible to identify the most important design parameters in reducing the carry-over of particulate material in this bottom-feed vessel. Because of the commercial nature of this study, all quantitative values of flow rates, concentrations and length and velocity scales have been replaced with reference to nominal (unspecified) values.

2. Mathematical model

Because low particle volume fractions are expected in the vessel, a drift-flux multi-phase model is chosen rather than a fully coupled multi-phase model. A literature review showed that drift-flux models have been used successfully in the study of settling tanks and clarifiers, [1–3]. A fully two-phase model was compared to the drift-flux model used in this study and, for a free-settling problem with solid loadings similar to those applicable in the current study, almost identical results were obtained. The drift-flux model used in this study has also been used to solve a rectangular settling tank problem for which limited experimental results are available [3]. There is good qualitative agreement.

The advantage of the drift-flux model is that six different particle sizes are included in the model. Each particle size is representative of one of the size classes measured in the plant data, and its value is set equal to the median particle size in the class. Using six particle sizes in a fully multi-phase calculation would have been computationally prohibitive, and would have been unlikely to produce more valid results for the system under consideration. Because of the small particle sizes, the slip velocities required in the drift-flux model are chosen to be the Stokes settling velocity for each particle size. Because of the low solids loadings, these slip velocities are used without considering any corrections for hindered settling.

In a vector form, the governing equations are written:

$$\nabla \cdot (\rho \mathbf{V}) = 0, \tag{1}$$

$$\frac{\partial(\rho \mathbf{V})}{\partial t} + \nabla \cdot (\rho \mathbf{V} \otimes \mathbf{V}) = \nabla \cdot (\mu_{\text{eff}} \nabla \mathbf{V}) - \nabla P + \mathbf{f}, \tag{2}$$

$$\frac{\partial(\rho \phi)}{\partial t} + \nabla \cdot (\rho \mathbf{V} \phi) = \nabla \cdot \left(\frac{\mu_{\text{eff}}}{\sigma_\phi} \nabla \phi \right) + S_\phi, \tag{3}$$

$$\frac{\partial(\rho C_i)}{\partial t} + \nabla \cdot (\rho(\mathbf{V} + \mathbf{V}_\mathbf{s}) C_i) = \nabla \cdot \left(\frac{\mu_{\text{eff}}}{\sigma_{C_i}} \nabla C_i \right) + S_{C_i}. \tag{4}$$

where $\mathbf{V}$, P and $\mathbf{V}_\mathbf{s}$ are the velocity vector, pressure and settling velocity vector respectively. C_i is the volume concentration of particle class i. The effective viscosity is μ_{eff} (and is the sum of molecular and turbulent viscosity) and the density is ρ. The body force $\mathbf{f}$ due to particle–fluid density difference is modelled using a Boussinesq approximation. Turbulence is modelled using a

standard $k-\epsilon$ model with wall functions applied at the first grid point near wall surfaces. Thus ϕ in Eq. (3) represents either k or ϵ and the non-dimensional number σ_ϕ defines the turbulent diffusivity of ϕ. The effect of particles on turbulence has not been considered in the current study as it is believed that the low solids loadings and comparatively small particle settling velocities have only a very small effect when compared to the high inflow turbulence levels.

All variables are defined at the supply inlet. A zero-gradient condition is applied at the outlets and the liquid flow rates are distributed with a predetermined ratio through the outlets. No deposition of particles to walls is assumed, i.e. a zero-gradient boundary condition for particle concentrations is used at solid walls.

For a two-dimensional and axisymmetric flow, $\mathbf{V} = V_r\mathbf{e}_r + V_z\mathbf{e}_z$. A finite volume technique based on the SIMPLEC algorithm [4] was used to solve the time-averaged multi-phase Navier–Stokes equations. The convection terms in the momentum equations are discretised using a second-order finite volume scheme (QUICK) for non-uniform grids [5], and a first-order upwind scheme is used for solid-fraction equations and the governing equations for turbulent kinetic energy and dissipation rate.

There are several ways to incorporate Eq. (4) into the SIMPLEC algorithm. One way is to consider the settling term as a source term [3] and the usual discretisation method of [6] can be used. The approach used here is to discretise Eq. (4) directly and to include the settling velocity in the convection term. Note that the velocity field $(\mathbf{V}+\mathbf{V_s})$ is not divergence free, so a continuity equation cannot be used in the discretisation of the convection/diffusion equation, as normally done, e.g. [6].

In Patankar's SIMPLE approach [6], the following discretisation equation is obtained for the particle concentrations:

$$a_P C_P = \sum_{\mathrm{nb}=1}^{N} a_{\mathrm{nb}} C_{\mathrm{nb}} + c_0, \tag{5}$$

where P represents the cell centre and nb the neighbouring points. (The number of neighbouring points N, the coefficients a_P, a_{nb}, and the source term c_0 of the discrete equation depend on the discretisation schemes used.) When the flow field is required to satisfy the continuity equation, the discretised continuity equation can be used to ensure the following desirable property:

$$a_P = \sum_{\mathrm{nb}=1}^{N} a_{\mathrm{nb}}. \tag{6}$$

With the governing equations for particle concentrations in the drift-flux model, the particle flow field does not satisfy the continuity equation, and the above property will not need to be ensured.

3. Computational domain

The physical geometry of the vessel is such that the feed inlet is centrally located at the base of the cone and issues vertically into the vessel. Overflow exits the roof of the vessel through a number of overflow pipes. Underflow is pumped out of one side of the vessel through a pipe located near the inflow. Because axisymmetry is used in the simulations reported here, the underflow pipe is treated as an annulus and the set of overflow pipes on the vessel roof is replaced by a central pipe and an overflow annulus at approximately half the radius of the vessel. The computational domain is shown in Fig. 1.

The domain is discretised on a non-uniform rectangular mesh using a cylindrical coordinate system. The geometry of the cone base of the vessel is included using a stair-step approximation.

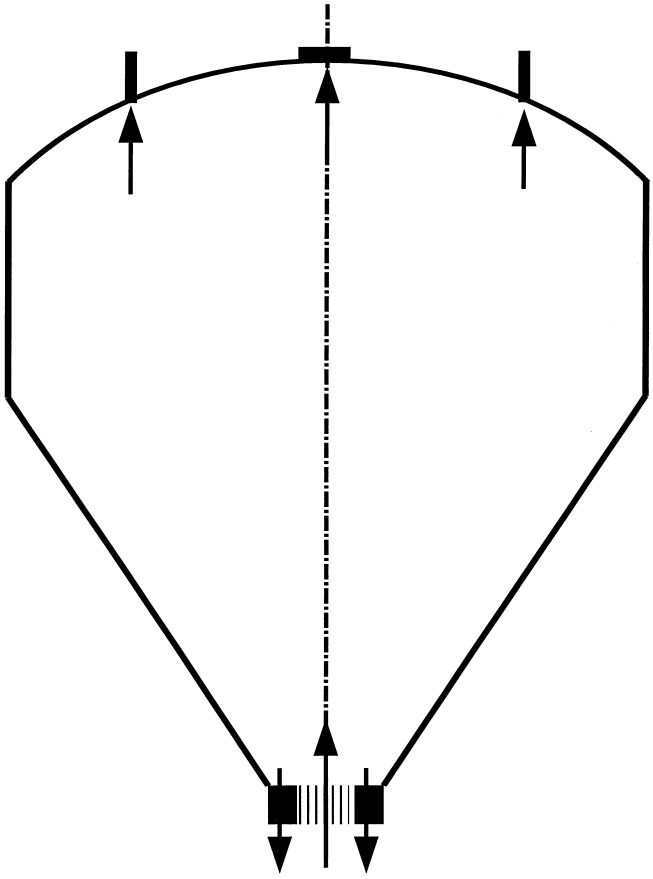

Fig. 1. Computational domain for the particle separation vessel.

An example of the computational mesh for the simulation of standard operating conditions is provided in Fig. 2 (47×71 grid points in total).

4. Validation against plant data

The numerical model was validated against data measured at the plant. The solid material has the same nominal density irrespective of particle size and the aim of the separation is to minimise the carry-over of particles with a size greater than d_m. Thus in all discussion below, particle sizes are described in terms of the maximum desirable particle size, d_m. The plant data was collected by sampling the feed, the underflow and the overflow and measuring the total solids and the percentage of the total solids in each of six different particle size classes.

A comparison between numerical prediction and measured data for both underflow and overflow are presented in Table 1. The percentage for each size class refers to the mass percentage of the total solids in the carry-over or under-flow that is greater than a given size (or smaller than the smallest size). (Note that the sum of the percentages for $d > \frac{1}{3}d_m$ and $d < \frac{1}{3}d_m$ must be 100%.) Statistical fluctuations in the plant data are believed to account for the majority of the discrepancies between measured and predicted results, and in general there is good agreement between prediction and measurement. The major exception is for the underflow of very large particles. It is

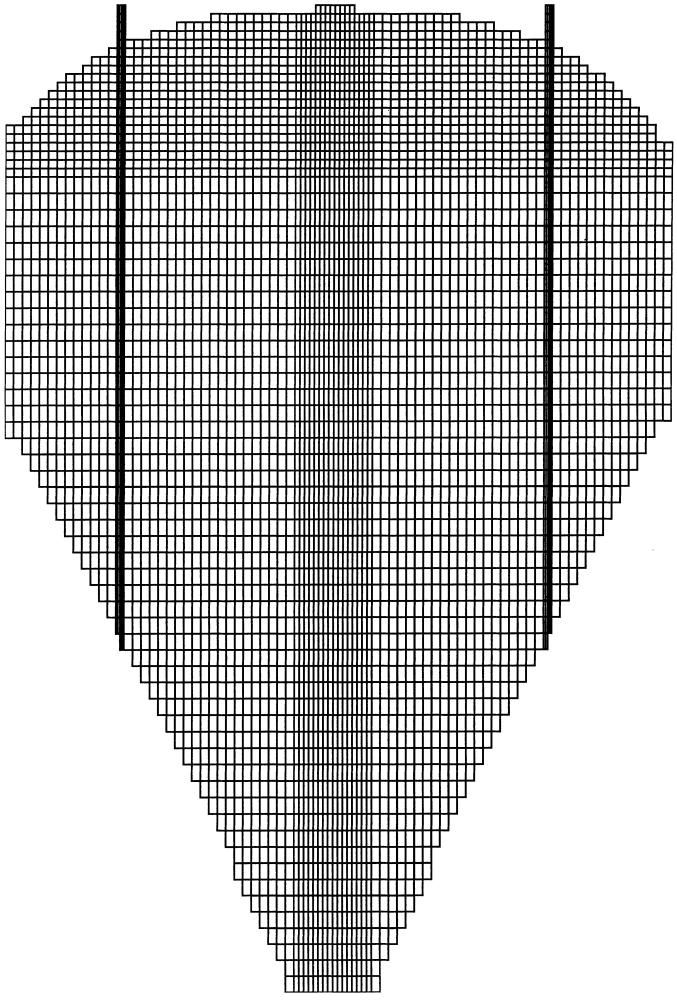

Fig. 2. Computational mesh used in simulation of standard operating geometry (reflected about the axis).

Table 1
Comparison between measured and predicted percentages of solids in the overflow and underflow for different particle sizes and the total volume fraction (TVF) of solids in the overflow and underflow

Particle size	$> 3d_m$	$> 1.5d_m$	$> d_m$	$> \frac{1}{2}d_m$	$> \frac{1}{3}d_m$	$< \frac{1}{3}d_m$	TVF
Overflow							
Measured %	0.7	1.5	11.3	26.3	33.6	66.4	0.0269
Predicted % (47 × 71)	0.0	0.2	8.5	23.7	31.7	68.3	0.0256
Predicted % (92 × 140)	0.0	0.1	7.6	22.7	30.7	69.3	0.0286
Underflow							
Measured %	27.4	59.2	69.9	76.0	78.7	21.3	0.0852
Predicted % (47 × 71)	19.0	51.2	64.2	72.8	75.9	24.1	0.0746
Predicted % (92 × 140)	18.3	50.5	64.9	73.7	76.8	23.2	0.0881

Predicted results are presented for the standard resolution (47 × 71) and fine resolution (92 × 140).

known that the plant measurement for this particle size class is definitely in error, thus this discrepancy is not a serious problem here.

In addition to the computation at the standard resolution of 47×71, a simulation of the base flow case was undertaken at a finer resolution of 92×140 in order to investigate grid dependence of the solution. The particle carry-over results for this case are also shown in Table 1, and indicate that reasonable, although not complete, grid independence has been obtained. Because of this, the results here are used to predict trends, rather than exact magnitudes, in the overflow and underflow of solids under various design modifications. The standard grid resolution is used for all computations in the remainder of the paper.

The data presented in Table 1 corresponds to standard operating conditions in the vessel, and the resulting flow is referred to below as the base flow. The distribution of volume fraction for the four larger particle size classes for this case are shown in Fig. 3. The volume fraction data for the two smallest classes show little variation throughout the vessel and may be considered to be uniformly distributed.

Flow streamlines and total volume fractions of solids are shown in Fig. 4, which illustrates the basic flow pattern observed for all flow configurations. The feed jet is laden with particles and is negatively buoyant with respect to the surrounding, particle-depleted fluid. Large particles settle out of the jet to the base of the cone and are withdrawn through the underflow, whereas smaller particles are more easily transported to the top of the vessel and out the overflow. At the top of the negatively buoyant jet, the flow is characterised by a recirculation which is sufficiently strong to suspend significant amounts of particles with $d > d_{\mathrm{m}}$. The effect of this recirculation on particles with $d > d_{\mathrm{m}}$ can be seen in Fig. 4 where the volume fraction of particles in the upper section of the vessel is higher at the outside of the vessel than it is on the centerline. This recirculation is responsible for the carry-over of a significant amount of large particles, despite the fact that the negatively buoyant feed jet stops well short of the overflow outlets.

5. Negatively buoyant jets

Before proceeding with a numerical study of different design variations, the basic flow pattern shown in Fig. 4 is discussed in some detail as it sheds light on later results.

It is useful to examine qualitatively the contours of the total volume fractions of solids for the base case during the establishment of the flow, see Fig. 5. Initially, the dense particle-laden jet penetrates the lighter surrounding fluid with entrainment, and reaches its initial maximum height at about 80 s. The jet top drops back at 100 s, due to its negative buoyancy. Throughout the initial stages of the jet development, there is a downward flow around the jet which carries particles down to the surrounding fluid, gradually increasing the mean density of the mixture in the conical base region. At about 200 s, a lower and quasi-steady jet height is established. The flows in both the jet and the surrounding fluid are fairly stable at 200 s. The jet height at 200 s is lower than that at 80 s, probably due to the fact that the particle–liquid mixture being entrained in the upward flow is heavier than the pure liquid that was previously entrained. Eventually (approximately 200 min) a steady state solution is achieved with a stable jet top that is much lower than the initial maximum height that occurred at about 80 s. There is a secondary recirculation zone above the jet top in the vessel, followed by an upward piston-type flow pattern towards the top outlets.

Baines et al. [7,8] described this type of flow as a 'fountain'. Their study suggested that in an open environment, the fountain height ($z_{\max}$) is a linear function of the Froude number (Fr):

$$\frac{z_{\max}}{R} = C\ \mathrm{Fr}, \tag{7}$$

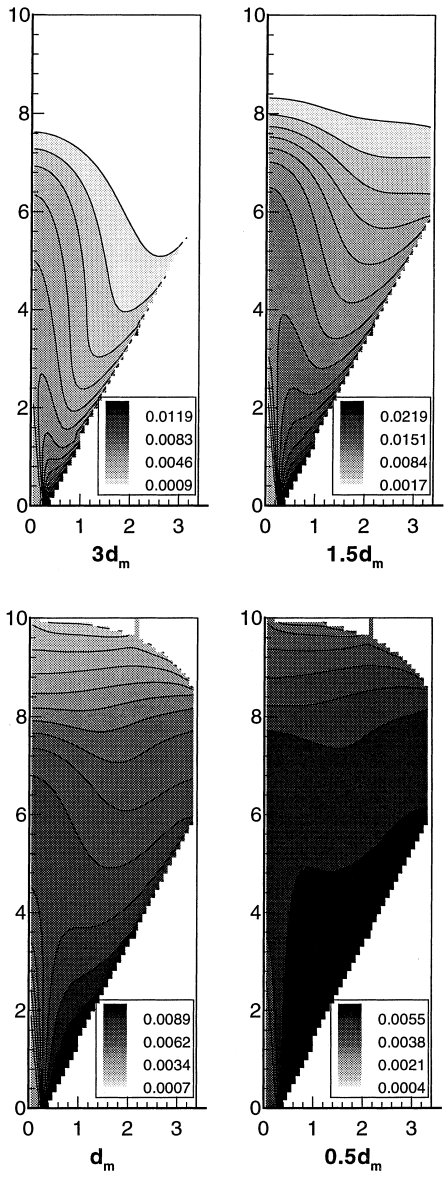

Fig. 3. Distribution of volume fractions of the four largest particle size classes.

where R is the radius of the feed inlet and C is a constant. The Froude number here is defined as

$$\mathrm{Fr} = \sqrt{\frac{\rho_s U_0^2}{(\rho_0 - \rho_s) R g}}, \tag{8}$$

where U_0 is the feed velocity, g the gravity acceleration, ρ_0 the feed fluid density and ρ_s the clear surrounding fluid density.

Although Eq. (7) is probably not directly applicable to fountains in an enclosure, the fountain height in the vessel here will be determined mainly by a Froude number. It will be shown later that the fountain height is a dominant design parameter in the particle carry-over performance in the vessel considered here. Eq. (7) suggests that for a constant feed flow rate, the most effective

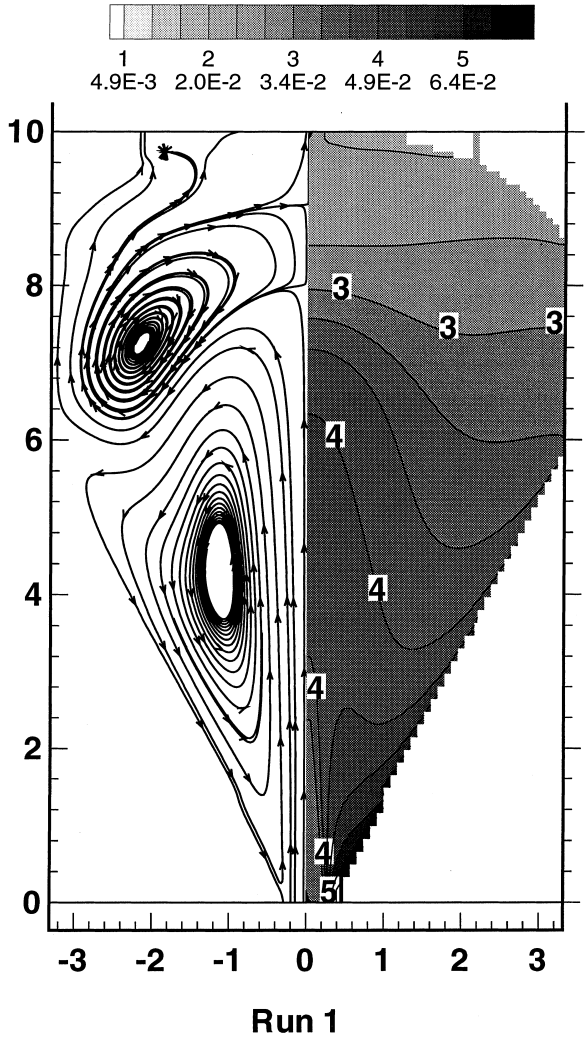

Fig. 4. Flow streamlines and contours of total volume fractions of solids for the base case.

method to reduce the fountain top height is to increase the feed inlet radius, R, which also reduces the feed velocity, U_0.

6. Effect of design modifications

Three design modifications were investigated with the aim of reducing the carry-over of solid particles larger than d_m (referred to below as 'large particles'). The three modifications were: an increase in vessel height; an increase in vessel diameter; and an increase in feed-pipe diameter. Each of these three modifications was a practical alternative given existing plant constraints, process down-time due to modification and cost.

6.1. Effect of increasing vessel height

Because the feed jet is a particle-laden, negatively buoyant jet, increasing the total height of the vessel may at first appear to be one way in which to reduce the large particle carry-over.

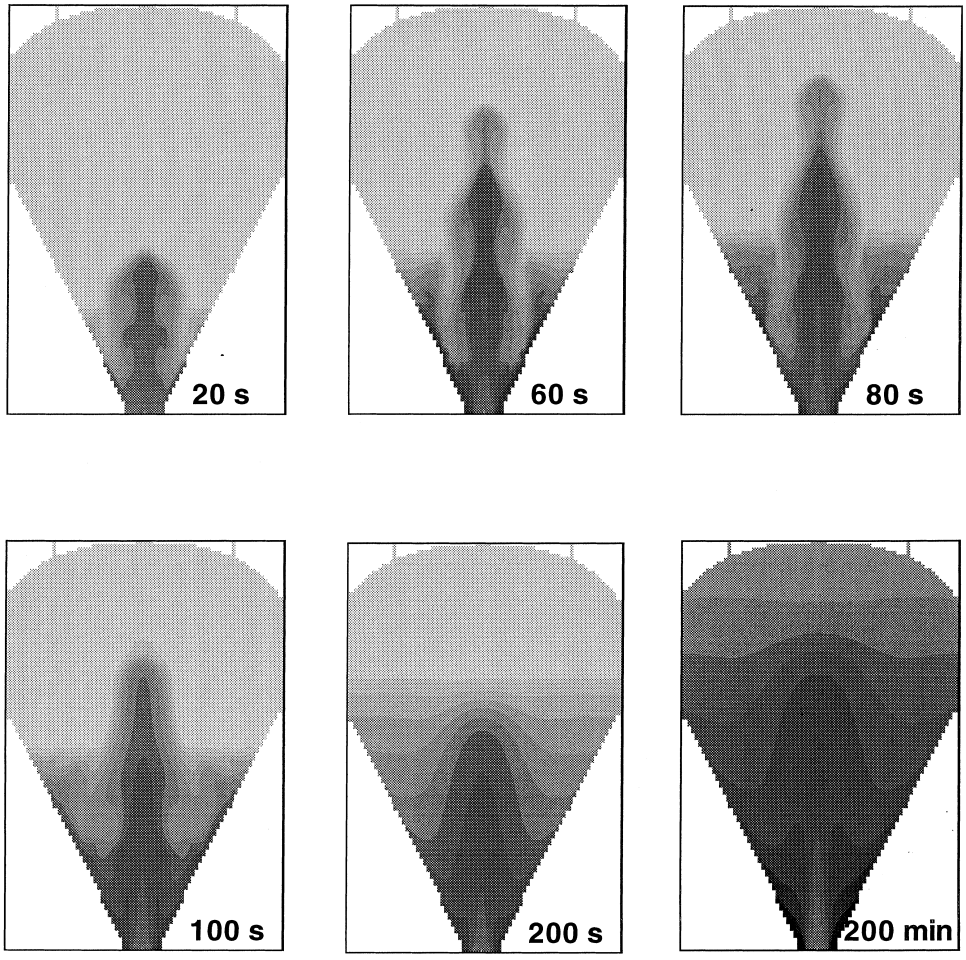

Fig. 5. Contours of total solids volume fractions for the base case during the establishment of the flow.

However, increasing the vessel height has little effect on the basic flow pattern, as seen in Fig. 6 in which the vessel height has been increased by 10%. Although the added height provides a longer 'upward journey' for particles and gives additional time for large particles to settle, results of carry-over suggest little difference, as seen in Table 2. The reason for this is due to the strength and orientation of the large recirculation at the top of the vessel. As the feed jet slows, it forms a fountain in which particles are dragged away from the axis and toward the outside of the vessel. This flow stagnates on the outer wall of the vessel with the majority of the new feed liquid flowing into the large recirculation in the upper part of the tank. Although some heavy particles are able to settle during the radial motion at the top of the feed jet, many are carried by the upper recirculation toward the outer overflow pipes. In order to significantly decrease the carry-over of large particles by increasing the vessel height, a significant increase would be required.

6.2. Effect of increasing vessel diameter

Two simulations were undertaken to investigate the effects of increasing the vessel diameter. The diameter was increased in such a way that the total vessel height and the angle of the conical

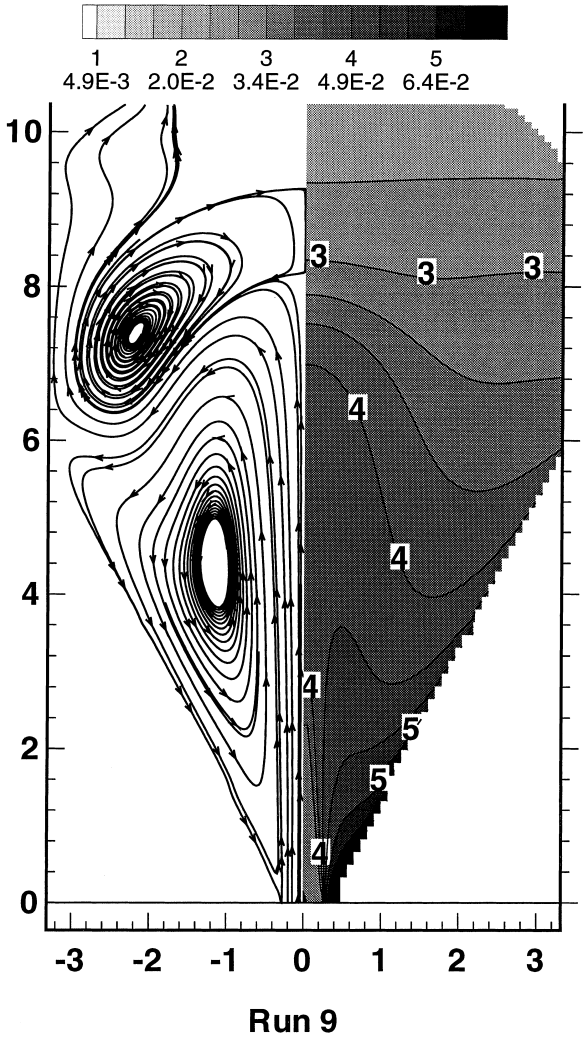

Fig. 6. Fluid flow streamlines and contours of total volume fractions of solids when vessel height is increased by 10%.

Table 2
Percentage carry-over and underflow for all particle sizes and total volume fraction of solids (TVF) in carry-over and underflow for different vessel heights

Particle size	$> 3d_m$	$> 1.5d_m$	$> d_m$	$> \frac{1}{2}d_m$	$> \frac{1}{3}d_m$	$< \frac{1}{3}d_m$	TVF
Overflow							
Base	0.0	0.2	8.5	23.7	31.7	68.3	0.0256
Base + 5%	0.0	0.1	8.2	26.3	31.6	68.4	0.0255
Base + 10%	0.0	0.0	7.4	22.7	30.8	69.2	0.0252
Underflow							
Base	19.0	51.2	64.2	72.8	75.9	24.1	0.0746
Base + 5%	18.5	51.0	65.0	73.6	76.6	23.4	0.0768
Base + 10%	18.3	50.6	65.2	73.8	76.8	23.2	0.0776

base were kept constant. An increase in diameter would reduce the mean fluid rise velocity in the top region of the vessel and on the basis of bulk flow quantities alone may be expected to reduce the carry over.

The superficial fluid rise velocity (V_R) in the top of the tank is calculated by dividing the total volumetric overflow by the cross-sectional area of the tank at maximum diameter. Writing the nominal settling velocity of particles of size d_m as V_d, the superficial rise velocity in the base case is $V_S^B = 0.8V_d$. When the tank diameter is increased by 15%, the superficial rise velocity $V_S^{15} = 0.61V_d$ and when it is increased by 30%, $V_S^{30} = 0.48V_d$. Thus an increase of 30% should be expected to reduce the carry-over of large particles significantly.

As in the case of increased vessel height, the basic flow pattern is not altered significantly when the vessel diameter is increased, as seen in Fig. 7 which is for an increase of 15%. There is a small improvement in the carry-over of large particles when the vessel diameter is increased, (see Table 3), although the improvements are far smaller than may be expected on the basis of accompanying reductions in superficial rise velocity. The reason this is the case is related to the flow pattern of fountain and recirculation-zone that is still present and is able to carry heavy particles from the jet outwards and upwards toward the outer overflow pipes.

6.3. Effect of increasing feed-pipe diameter

Increasing the feed-pipe diameter has the most dramatic effect on the flow patterns and solids distribution, as seen in Table 4 and Fig. 8 (for an increase of 100%). Because of the lower supply velocity of the particle-laden, negatively buoyant jet, it attains a significantly lower height than the base case before the familiar fountain pattern appears and the jet is deflected away from the axis and toward the vessel walls. The upper recirculation region is also reduced considerably in strength and size.

This design alteration also significantly reduces the carry-over of large particles, (see Table 4). This result is despite the fact that the superficial rise velocity of the fluid in the top of the tank is not altered by decreasing the feed jet velocity. This result is related to the reduction in size and strength of the upper recirculation which is unable to easily lift as many large particles out and upwards toward the outer overflow pipes.

The reduction in height of the supply jet is the single most important factor in reducing the carry-over of large particles, and is the design change that is recommended.

7. Summary

The major findings of this numerical study are that the predicted flow patterns in the particle separator show that the particle-laden supply flow stream is a negatively buoyant jet. The fountain-type behaviour of this jet causes a large recirculation in the upper part of the tank that is the primary factor in determining the carry-over of large particles. The height the negatively buoyant jet attains is an important factor in determining the size and strength of the upper recirculation and is thus an important factor in determining the overall performance of the separator. Higher jets give larger and stronger recirculation which in turn causes higher carry-over (poorer performance). The maximum jet height depends critically on the inlet velocity and the most effective way of reducing feed velocity (at the same time as keeping throughput constant) is to increase the inlet diameter. Increasing the overall height or diameter of the separator is far less effective in reducing the carry-over over the range of variation considered.

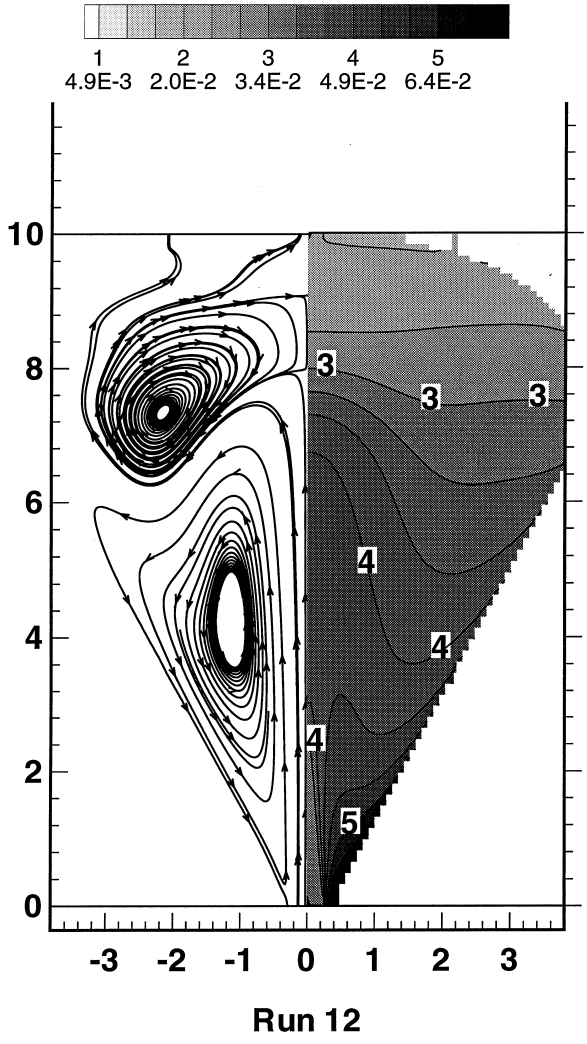

Fig. 7. Fluid flow streamlines and contours of total volume fractions of solids when the vessel diameter is increased by 15%.

Table 3
Percentage carry-over and underflow for all particle sizes and total volume fraction of solids (TVF) in carry-over and underflow for different vessel diameters

Particle size	$> 3d_m$	$> 1.5d_m$	$> d_m$	$> \frac{1}{2}d_m$	$> \frac{1}{3}d_m$	$< \frac{1}{3}d_m$	TVF
Overflow							
Base	0.0	0.2	8.5	23.7	31.7	68.3	0.0256
Base + 15%	0.0	0.1	7.8	23.0	31.0	69.0	0.0253
Base + 30%	0.0	0.1	6.9	22.0	30.1	69.9	0.0250
Underflow							
Base	19.0	51.2	64.2	72.8	75.9	24.1	0.0746
Base + 15%	18.4	50.7	64.9	73.7	76.7	23.3	0.0772
Base + 30%	18.2	50.2	65.0	73.8	76.9	23.1	0.0780

Table 4
Percentage carry-over and underflow for all particle sizes and total volume fraction of solids (TVF) in carry-over and underflow for different feed pipe diameters

Particle size	$> 3d_m$	$> 1.5d_m$	$> d_m$	$> \frac{1}{2}d_m$	$> \frac{1}{3}d_m$	$< \frac{1}{3}d_m$	TVF
Overflow							
D	0.0	0.2	8.5	23.7	31.7	68.3	0.0256
1.5*D*	0.0	0.0	5.3	20.4	28.7	71.3	0.0244
2.0*D*	0.0	0.0	3.2	18.0	26.5	73.5	0.0237
Underflow							
D	19.0	51.2	64.2	72.8	75.9	24.1	0.0746
1.5*D*	17.8	49.3	65.3	74.3	77.3	22.7	0.0796
2.0*D*	17.4	48.2	65.4	74.8	77.7	22.8	0.0814

The feed pipe diameter of the base case is *D*.

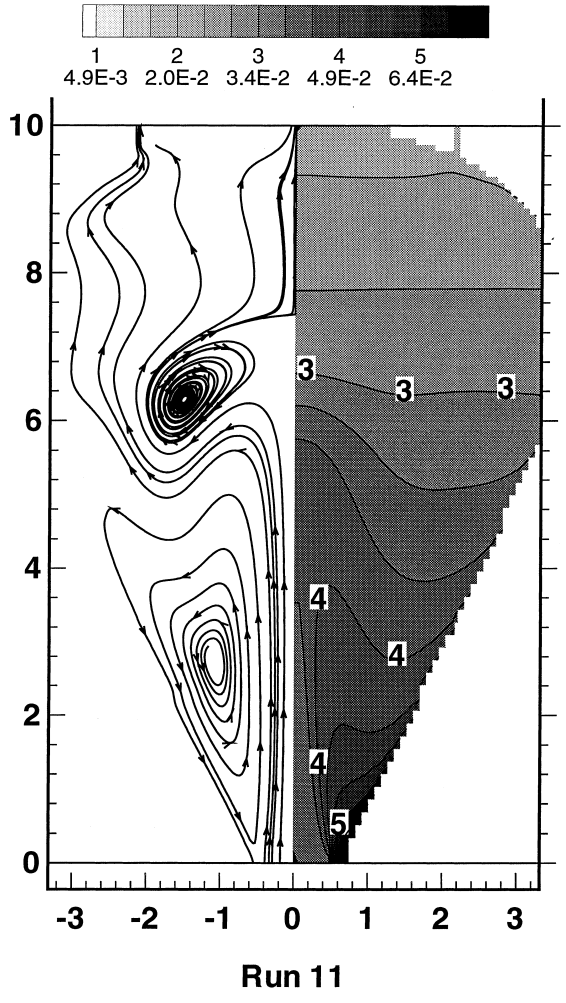

Fig. 8. Fluid flow streamlines and volume fraction contours with increased feed-pipe diameter.

Nomenclature

C_i	Volume fraction of particle class i
d_{m}	Cut-off particle size
Fr	Froude number
$\mathbf{f}$	Body force
g	Gravity acceleration
$\mathbf{e}_r$	Unit radial vector
$\mathbf{e}_z$	Unit axial vector
k	Turbulent kinetic energy
P	Pressure
R	Feed inlet radius
S_ϕ	Source term for ϕ
U_0	Feed velocity
$\mathbf{V}$	Liquid velocity
$\mathbf{V_s}$	Particle slip velocity
V_d	Settling velocity of particles with size d_{m}
V_{R}	Superficial rise velocity in the top of the tank
$z_{\max}$	Fountain height
ϵ	Turbulent dissipation
μ_{eff}	Total effective mixture viscosity
ϕ	Turbulent scalar (either k or ϵ)
ρ	Liquid density
ρ_0	Feed mixture density
ρ_s	Clear surrounding fluid density
σ_{C_i}	Prandtl number of diffusion of particle class i
σ_ϕ	Prandtl number of diffusion of ϕ

References

[1] I. Celik, W. Rodi, Modelling suspended sediment transport in non-equilibrium situations, Journal of Hydraulic Engineering 114 (1989) 1157–1191.
[2] E.W. Adams, W. Rodi, Modelling flow and mixing in sedimentation tanks, Journal of Hydraulic Engineering 116 (1989) 895–913.
[3] S. Zhou, J.A. McCorquodale, Modelling of rectangular settling tanks, Journal of Hydraulic Engineering 118 (1992).
[4] J.P. Van Doormaal, G.D. Raithby, Enhancement of the SIMPLE method for predicting incompressible fluid flows, Numer. Heat Transfer 7 (1984) 147–163.
[5] Y. Li, M. Rudman, Assessment of higher-order upwind schemes incorporating FCT for convection dominated problems, Numer. Heat Transfer B 27 (1995) 1–21.
[6] S.K. Patankar, Numerical Heat Transfer and Fluid Flow, Hemisphere, Washington DC, 1980.
[7] W.D. Baines, J.S. Turner, I.H. Campbell, Turbulent fountains in an open chamber, Journal of Fluid Mechanics 212 (1990) 557–592.
[8] W.D. Baines, A.F. Corriveau, T.J. Reedman, Turbulent fountains in a closed chamber, Journal of Fluid Mechanics 255 (1993) 621–646.